Mathematical Sciences Exercise Answer Part II

Baiyuan Chen *

The University of Tokyo

Contents

*Email: chenbaiyuan75@gmail.com

2 Monte Carlo Method

2.1 Random Number Generation

2.1.1 Exercise 2.1.1

1.&2. Generate uniformly distributed random numbers in [0, 1) using the linear congruential method and plot the histogram.
Using the linear congruential method with $a = 1229, c = 351750, m = 1664501$, the generated uniform random numbers are shown in Figure 1.

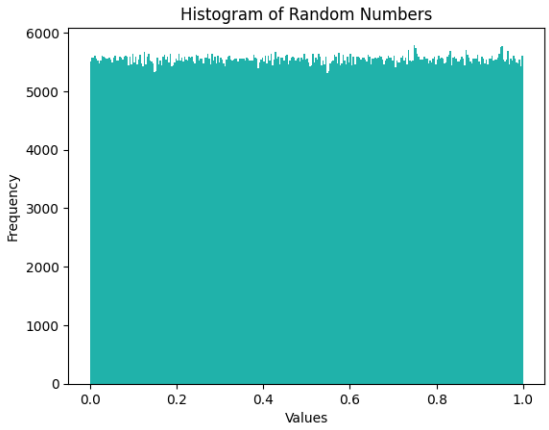

Figure 1: Histogram of generated uniform random numbers

3. Calculate the mean, deviation, and correlation of two consecutive variables.
The calculated mean is 0.5003, deviation is 0.2888, and the correlation of two consecutive variables is 0.0008.

4. Generate random numbers that follow the probability density function

$$\rho(x) = \begin{cases} 1 - |x| & (|x| \leq 1) \\ 0 & (|x| \geq 1) \end{cases}$$

.
Random numbers are generated using the inverse transform method. The cumulative distribution function (CDF) of the above probability density function (PDF) is

$$F(x) = \begin{cases} 0 & (x < -1) \\ \frac{(x+1)^2}{2} & (-1 \leq x \leq 0) \\ \frac{-x^2+2x+1}{2} & (0 < x < 1) \\ 1 & (x \geq 1) \end{cases} \tag{1}$$

Both graphs are shown in Figure 2 on the left, while the histogram of random numbers generated based on the inverse function is shown on the right. This corresponds to the shape of the PDF, meaning more random numbers are generated where the probability is higher and fewer where it is lower.

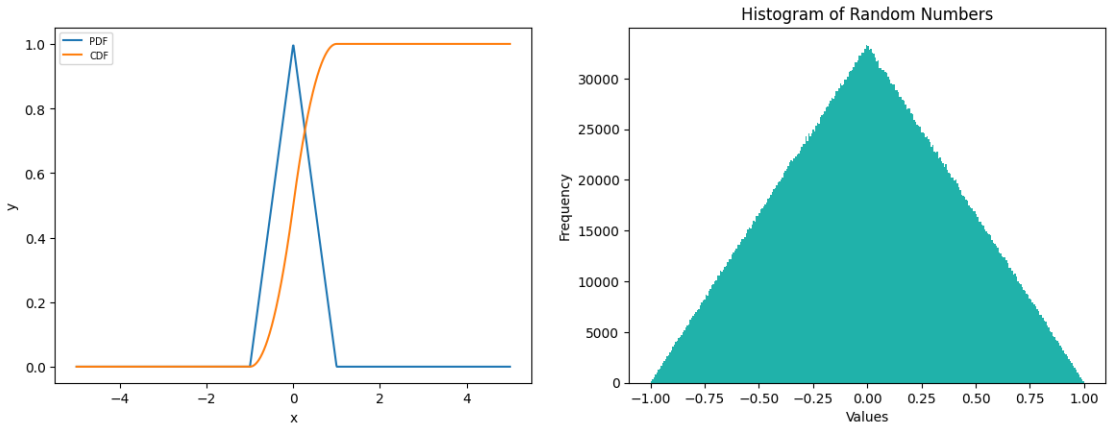

Figure 2: Probability Density Function (PDF), Cumulative Distribution Function (CDF), and Histogram of Random Numbers Following PDF

5. Devise an algorithm to generate random numbers following an arbitrary probability density function (with finite support).
An algorithm using uniform random numbers and the inverse transform method:

1. Define the probability density function $f(x)$.
2. Calculate the cumulative distribution function $F(x) = \int_{-\infty}^{x} f(t)dt$.
3. Find the inverse function of the cumulative distribution function $F^{-1}(x)$.
4. Generate a uniform random number U from 0 to 1 and compute $F^{-1}(U)$.

Thus, random numbers $X = F^{-1}(U)$ following an arbitrary PDF $f(x)$ can be obtained.

6. Use random numbers to numerically compute the value of an integral. As an example, write a program that approximates the value of π using random numbers.
The area of a circle is calculated as πr^2, so we focus on a quarter of a circle on a 1×1 square. The algorithm:

1. Randomly generate 10^7 points within the 1×1 square.
2. Count the number of points that satisfy $x^2 + y^2 \leq 1$, denoted as q.
3. Calculate $\pi = 4q$.

The result of the calculation is shown in Figure 3, with π approximated as 3.1422.

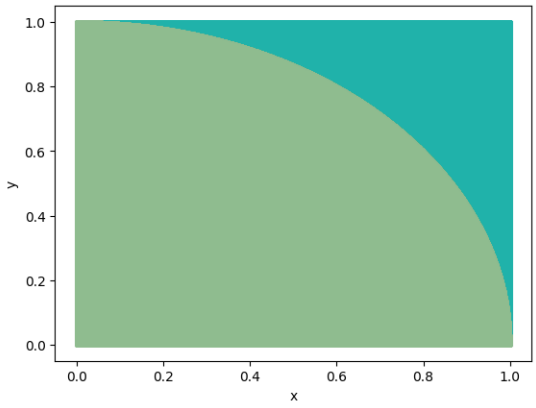

Figure 3: Calculation of π

2.2 Random Walk

2.2.1 Exercise 2.2.1

1. Implement a random walk to observe the behavior of a "drunkard's" movement. Calculate the probability $p(m, n)$ that the drunkard is at position m at step n (plot $\log p(m, 100)$ against m^2). How does the mean squared displacement behave with respect to n?
Three random walks were implemented, and the results are shown in Figure 4. The relationship between $\log p(m, 100)$ and m^2 is depicted in Figure 5.

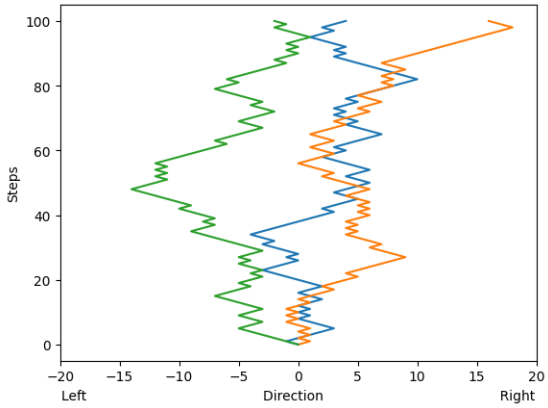

Figure 4: Random Walk

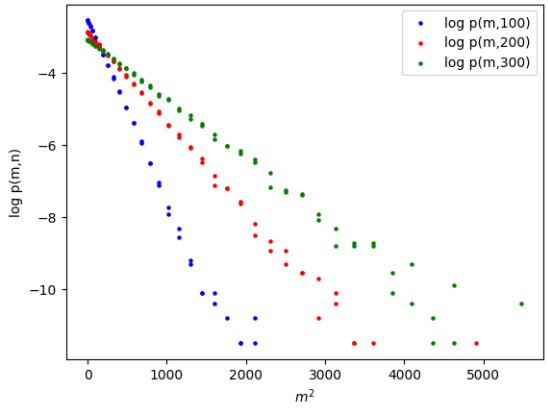

Figure 5: Relationship between $\log p(m, 100)$ and m^2

2. A simple and approximate method for generating a Gaussian distribution involves generating k uniformly distributed random numbers in $[0, 1)$, summing them, and dividing the sum by k. Generate random numbers following this approximate Gaussian distribution using this method and compare the distribution with $p(m, 100)$. How does the shape of the distribution change as k increases? Discuss why this method approximates the Gaussian distribution.

Following the given method, the histogram of random numbers generated with $k = 12$ is shown in Figure 6. The distribution of $p(m, 100)$ is shown in Figure 7, and both are similar. The histograms for $k = 2$, 5, 8 are shown in Figure 8, where the distribution becomes smoother and gradually closer to the Gaussian distribution as k increases. (Histograms for $k > 12$ are omitted due to minimal differences with $k = 12$.)

The reason that the mean of uniformly distributed random numbers approximates the Gaussian distribution is due to the Central Limit Theorem, which states that the sum of a large number of independent and identically distributed random variables converges to a Gaussian distribution, regardless of their original distribution. Since the uniform distribution assigns equal probability to all values within a specific range, the mean of uniform random numbers converges to a Gaussian distribution by the Central Limit Theorem.

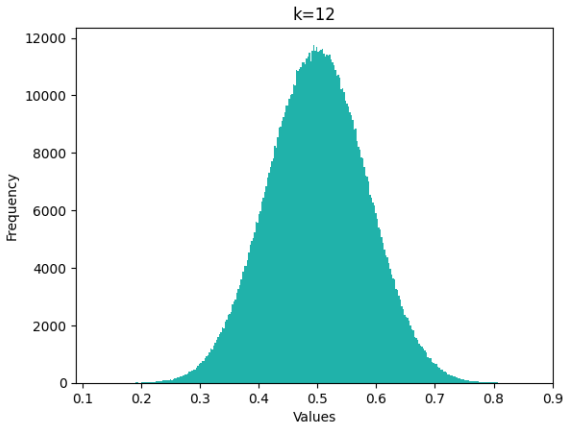

Figure 6: Histogram of Random Numbers Following Gaussian Distribution Created from Sum of Uniform Distributions

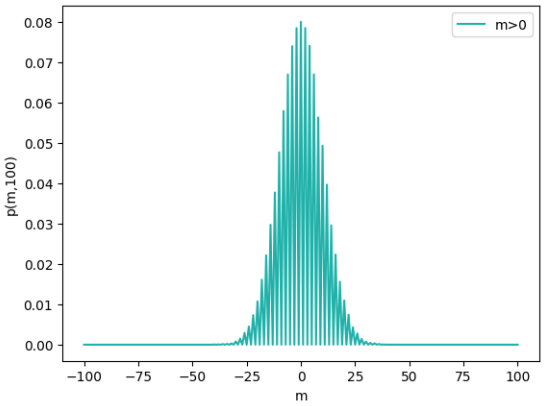

Figure 7: Distribution of $p(m, 100)$

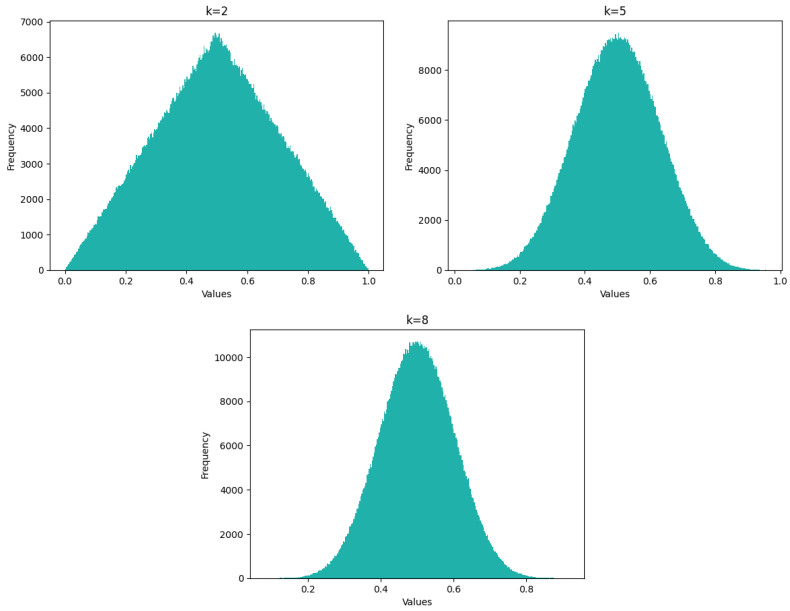

Figure 8: Histograms for $k = 2$, 5, 8

3. Let x, y be uniformly distributed random numbers in $[0, 1)$. Then, the variables

$$X = \sqrt{-1 \log(1 - x)} \cos(2\pi y)$$

$$Y = \sqrt{-1 \log(1 - x)} \sin(2\pi y)$$

both follow the Gaussian distribution $\rho(X) = \frac{1}{\sqrt{2\pi}} e^{-\frac{X^2}{2}}$. Demonstrate this analytically. Also, generate random numbers using the Box-Muller method and compare with both the summation method and the distribution of $p(m, 100)$.

Since x is a uniformly distributed random number in $[0, 1)$, $1 - x$ can be replaced by x in X and Y. Let $z = -2 \log x$, then

$$X = \sqrt{z} \sin 2\pi x, \; Y = \sqrt{z} \cos 2\pi y \;\Rightarrow\; X^2 + Y^2 = z = -2 \log x \;\Rightarrow\; x = e^{-\frac{X^2+Y^2}{2}} \tag{2}$$

holds true. Thus,

$$\frac{\partial X}{\partial x} = -\frac{\sin 2\pi y}{x\sqrt{x}}, \quad \frac{\partial Y}{\partial x} = -\frac{\cos 2\pi y}{x\sqrt{z}}, \quad \frac{\partial X}{\partial y} = 2\pi\sqrt{z} \cos 2\pi y, \quad \frac{\partial Y}{\partial y} = -2\pi\sqrt{z} \sin 2\pi y \tag{3}$$

can be derived. Using these, we can transform the probability density function.

If the probability density functions of X, Y are denoted as p_{XY} and that of x, y as p_{xy}, then $p_{XY}\Delta(XY) = p_{xy}\Delta(xy)$ holds true, where $\Delta(xy)$ is the infinitesimal area formed by $(x, y), (x + \Delta x, y), (x, y + \Delta y), (x+\Delta x, y+\Delta y)$, and $\Delta(XY)$ is the infinitesimal area of the parallelogram formed by $(X, Y), (X + \frac{\partial X}{\partial x}\Delta x, Y + \frac{\partial Y}{\partial x}\Delta x), (X + \frac{\partial X}{\partial y}\Delta y, Y + \frac{\partial Y}{\partial y}\Delta y), (X + \frac{\partial X}{\partial x}\Delta x + \frac{\partial X}{\partial y}\Delta y, Y + \frac{\partial Y}{\partial x}\Delta x + \frac{\partial Y}{\partial y}\Delta y)$. The area of the parallelogram is equal to the magnitude of the cross product of two sides, so

$$\begin{aligned}\Delta(XY) &= |\frac{\partial X}{\partial x}\Delta x\frac{\partial Y}{\partial y}\Delta y - \frac{\partial X}{\partial y}\Delta y\frac{\partial Y}{\partial x}\Delta x| \\ &= |\frac{\partial X}{\partial x}\frac{\partial Y}{\partial y} - \frac{\partial X}{\partial y}\frac{\partial Y}{\partial x}|\Delta x\Delta y \\ &= |\frac{\partial X}{\partial x}\frac{\partial Y}{\partial y} - \frac{\partial X}{\partial y}\frac{\partial Y}{\partial x}|\Delta(xy)\end{aligned} \tag{4}$$

holds true. Substituting equation (3), $\frac{\Delta(XY)}{\Delta(xy)} = |\frac{2\pi}{x}| = \frac{2\pi}{x}$ holds. Therefore, $p_{XY} = \frac{x}{2\pi}p_{xy}$.

Since x, y are uniformly distributed random numbers in $[0, 1)$, $p_{xy} = 1$ within this range. Thus, $p_{XY} = \frac{x}{2\pi} = \frac{1}{2\pi}e^{-\frac{X^2+Y^2}{2}} = \frac{1}{\sqrt{2\pi}}e^{-\frac{X^2}{2}} \cdot \frac{1}{\sqrt{2\pi}}e^{-\frac{Y^2}{2}}$ holds true. Since X, Y are independent, both follow the Gaussian distribution $\rho(X) = \frac{1}{\sqrt{2\pi}}e^{-\frac{X^2}{2}}$.

From numerical calculations, the histogram of X and Y is shown in Figure 9, which matches the Gaussian distribution (Figure 10).

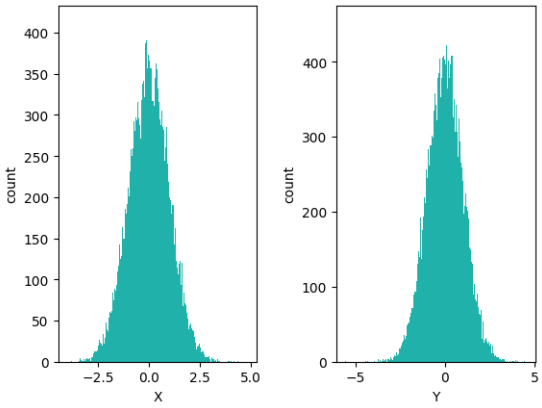

Figure 9: Histogram of Random Numbers Generated by the Box-Muller Method

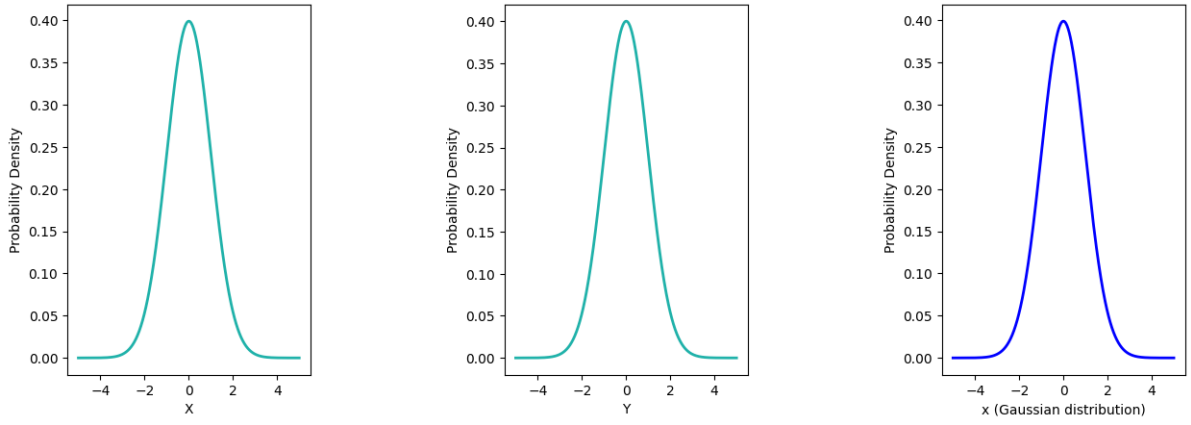

Figure 10: Probability Density Functions of X, Y (Left, Center) and Gaussian Distribution (Right)

4. When performing a Taylor expansion of the difference equation $p(x,t+\Delta t) = p(x-\Delta x,t)/2+p(x+\Delta x,t)/2$, what expression results? Use this to numerically solve the diffusion equation.

Expanding the left side of $p(x,t+\Delta t) = p(x-\Delta x,t)/2 + p(x+\Delta x,t)/2$ with respect to Δt and the right side with respect to Δx yields

$$\begin{aligned} p(x,t+\Delta t) &= p(x,t) + \Delta t\frac{\partial p}{\partial t}(x,t) + \mathcal{O}(\Delta t)^2 \approx p(x,t) + \Delta t\frac{\partial p}{\partial t}(x,t) \\ (p(x-\Delta x,t) + p(x+\Delta x,t))/2 &= p(x,t) + \frac{(\Delta x)^2}{2}\frac{\partial^2 p}{\partial x^2}(x,t) + \mathcal{O}(\Delta x)^2 \approx p(x,t) + \frac{(\Delta x)^2}{2}\frac{\partial^2 p}{\partial x^2}(x,t) \\ \Longrightarrow \qquad \frac{\partial p}{\partial t}(x,t) &= \frac{(\Delta x)^2}{\Delta t}\frac{\partial^2 p}{\partial x^2}(x,t) \end{aligned} \tag{5}$$

Thus, by setting the initial state to $u = \begin{cases} 1, & |x| \le 0.2 \\ 0, & otherwise \end{cases}$ and $\frac{(\Delta x)^2}{\Delta t} = 0.5$, the time evolution of the diffusion equation is shown in Figure 11.

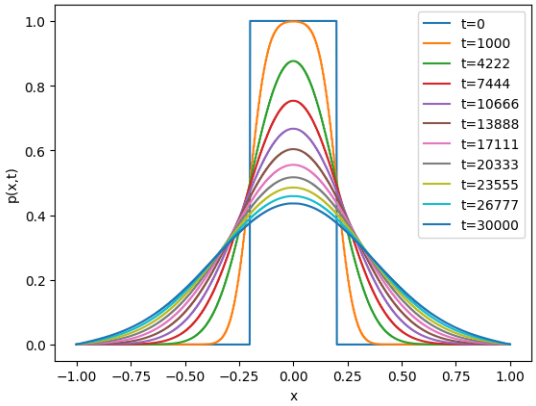

Figure 11: Diffusion Equation

2.3 Langevin Equation

2.3.0 Exercise 2.3.0

1. Implement the Langevin equation when $U(x) = 0$. When discretizing time, consider how ξ scales with the time step Δt. In this case, the particle simply diffuses, and the function $P(x)$ representing the probability of the particle's position follows the diffusion equation $\frac{\partial P(x)}{\partial t} = D\frac{\partial^2 P(x)}{\partial x^2}$. Perform numerical calculations. What is the diffusion coefficient D?

The diffusion coefficient D in the diffusion equation is $\frac{(\Delta x)^2}{\Delta t}$, as shown in equation (5). This means that if D increases, the change in x per unit time becomes larger, resulting in faster diffusion of the substance. Conversely, if D is small, the substance diffuses slowly. When implemented, the results are shown in Figure 12, indicating that as D increases, the diffusion rate becomes faster.

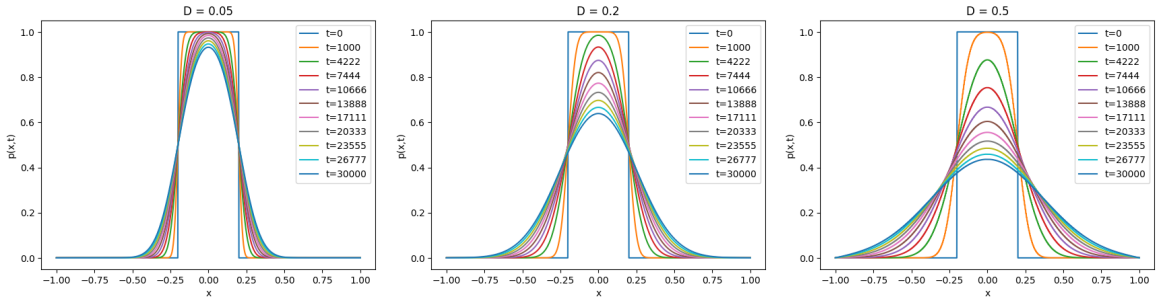

Figure 12: Diffusion Equation with $D = 0.05, 0.2, 0.5$

Next, calculate D numerically. When $U(x) = 0$,

$$\frac{dx}{dt} = \frac{p}{m}, \quad \frac{dp}{dt} = -\gamma p + \xi(t) \tag{6}$$

yields $m\frac{d^2x}{dt^2} = -\gamma m\frac{dx}{dt} + \xi(t) \quad (\langle \xi(t) \rangle = 0)$. Multiplying both sides by x and taking the time average gives

$$m\langle x\frac{d^2x}{dt^2}\rangle = -\gamma m\langle x\frac{dx}{dt}\rangle \tag{7}$$

Furthermore,

$$x\frac{dx}{dt} = \frac{1}{2}\frac{d(x^2)}{dt}, \quad x\frac{d^2x}{dt^2} = \frac{1}{2}\frac{d^2(x^2)}{dt^2} - \left(\frac{dx}{dt}\right)^2 \tag{8}$$

Thus, equation (7) becomes

$$\frac{1}{2}m\frac{d^2\langle x^2\rangle}{dt^2} - m\langle\left(\frac{dx}{dt}\right)^2\rangle = -\frac{1}{2}\gamma m\frac{d\langle x^2\rangle}{dt} \tag{9}$$

and since $\frac{1}{2}m\langle\left(\frac{dx}{dt}\right)^2\rangle = \frac{k_BT}{2}$,

$$\frac{1}{2}m\frac{d^2\langle x^2\rangle}{dt^2} - k_BT = -\frac{1}{2}\gamma m\frac{d\langle x^2\rangle}{dt} \tag{10}$$

Considering $\langle x^2\rangle$ as an ordinary differential equation, its solution is

$$\langle x^2\rangle = \frac{2kT}{m\gamma^2}(\gamma t + e^{-\gamma t} - 1) \tag{11}$$

For sufficiently large t, $\langle x^2\rangle = \frac{2kT}{m\gamma}t$. From the diffusion equation, $\langle x^2\rangle = 2Dt$, so $D = \frac{kT}{m\gamma}$.

2. Vary $U(x)$ and confirm that it follows the canonical distribution.

The Langevin equation and canonical distribution are shown on the left side of Figures 13 to 15. Adjusting T to an appropriate value ($T = 0.05K$), it can be observed that the Langevin equation follows the canonical distribution (right side of Figures 13 to 15).

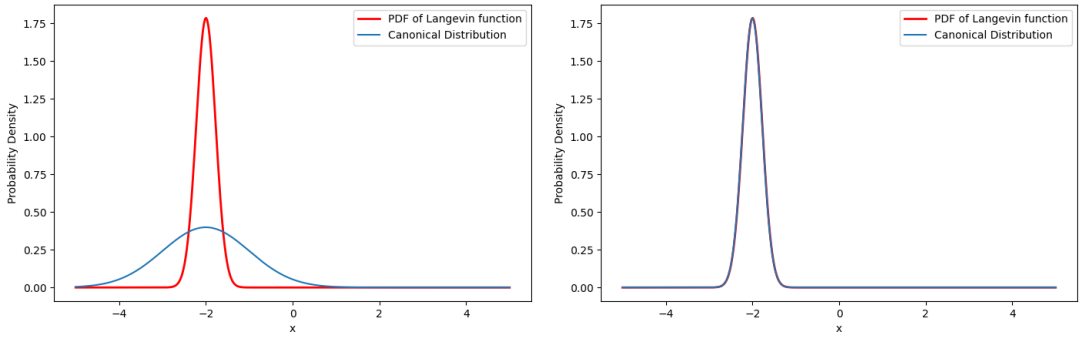

Figure 13: Probability Density Function (PDF) of the Langevin Equation and Canonical Distribution ($U(x) = 2x$)

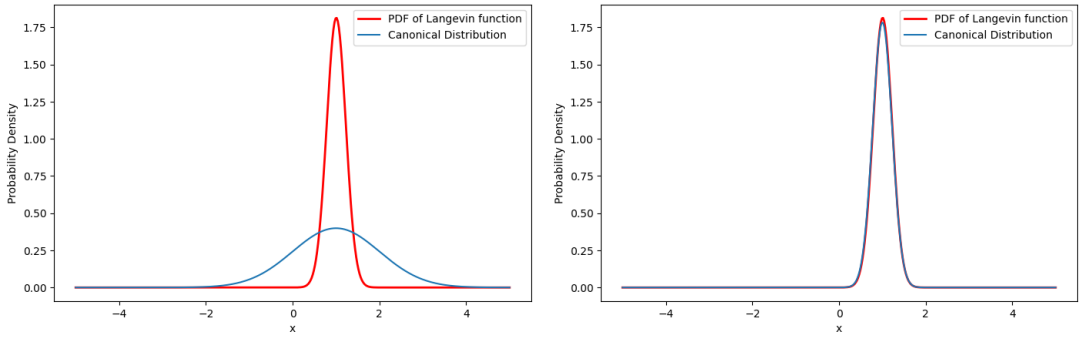

Figure 14: Probability Density Function (PDF) of the Langevin Equation and Canonical Distribution ($U(x) = -x$)

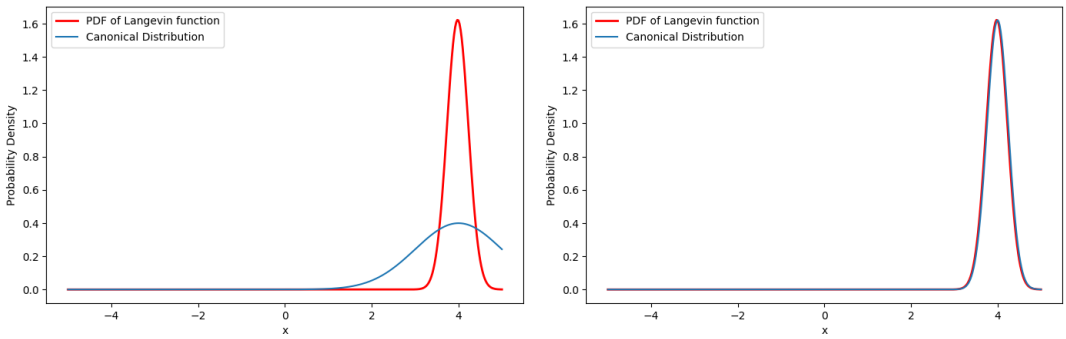

Figure 15: Probability Density Function (PDF) of the Langevin Equation and Canonical Distribution ($U(x) = -4x$)

2.5 Ising Model

2.5.0 Exercise 2.5.0: Demonstrate a non-trivial equality using equations.

Energy per site $u = \frac{1}{N}\langle H\rangle = \frac{1}{N}(-\frac{1}{Z}\frac{\partial Z}{\partial \beta})$**:**

$$\begin{aligned}\frac{1}{N}\langle H\rangle &= \frac{1}{N}\cdot Z^{-1}\sum_{\{S_i\}\mathcal{C}} e^{-\beta H(\{S_i\})} \\ &= -\frac{1}{NZ}\sum_{\{S_i\}\in\mathcal{C}}\frac{\partial}{\partial\beta}e^{-\beta H(\{S_i\})} \\ &= \frac{1}{N}(-\frac{1}{Z}\frac{\partial Z}{\partial\beta}).\end{aligned} \tag{12}$$

Specific heat per site $c = \frac{\partial\langle u\rangle}{\partial T} = \frac{1}{Nk_BT^2}(\langle H^2\rangle - \langle H\rangle^2)$**:**
For simplification, let $H(\{S_i\})$ be H, and $\sum_{\{S_i\}\in\mathcal{C}}$ be $\sum$.
From $u = \frac{1}{N}\langle H\rangle = \frac{1}{NZ}\sum He^{-\beta H}$ and $\langle H^2\rangle - \langle H\rangle^2 = \frac{1}{k_BT}(\sum H^2e^{-\beta H} - \frac{1}{Z}\sum H^2e^{-\beta H}He^{-\beta H})$, we get

$$\begin{aligned}\frac{\partial\langle u\rangle}{\partial T} &= \frac{\partial}{\partial T}(\frac{1}{Z}\sum ue^{-\beta H}) \\ &= \frac{\partial}{\partial T}\{\frac{1}{NZ}\sum(\sum He^{-\beta H})e^{-\beta H}\} \\ &= \frac{\partial}{\partial T}\{\frac{1}{NZ}(\sum He^{-\beta H})(\sum e^{-\beta H})\} \\ &= \frac{1}{N}\frac{\partial}{\partial T}(\frac{1}{Z}\sum He^{-\beta H}) \\ &= \frac{1}{N}\{-\frac{1}{Z^2}(\sum\frac{\partial\beta}{\partial T}\cdot\frac{\partial}{\partial\beta}e^{-\beta H})(\sum He^{-\beta H}) + \frac{1}{Z}\sum H\frac{\partial\beta}{\partial T}\cdot\frac{\partial}{\partial\beta}e^{-\beta H}\} \\ &= \frac{1}{N}\{\frac{1}{Z}\sum\frac{1}{k_BT^2}H^2e^{-\beta H} - \frac{1}{Z^2k_BT}(\sum He^{-\beta H})^2\} \\ &= \frac{1}{Nk_BT^2}\{\frac{1}{Z}\sum H^2e^{-\beta H} - \frac{1}{Z^2}(\sum He^{-\beta H})^2\} \\ &= \frac{1}{Nk_BT^2}(\langle H^2\rangle - \langle H\rangle^2).\end{aligned} \tag{13}$$

Magnetic susceptibility per site $\chi = \frac{\partial\langle s\rangle}{\partial h} = \frac{N}{k_BT}(\langle s^2\rangle - \langle s\rangle^2)$**:**
Given $H = -J\sum_{i,j}S_iS_j$ and $s = \frac{1}{N}\sum_{i=1}^{N}S_i$, we find that $s = -\frac{1}{N}\frac{\partial H}{\partial h}$.
Furthermore, from $\langle s^2\rangle - \langle s\rangle^2 = \frac{1}{Z}\sum s^2e^{-\beta H} - \frac{1}{Z^2}(\sum se^{-\beta H})^2$, we get

$$\begin{aligned}\frac{\partial\langle s\rangle}{\partial h} &= \frac{\partial}{\partial h}(\frac{1}{Z}\sum se^{-\beta H}) \\ &= \frac{1}{Z}(\sum s\frac{\partial H}{\partial h}\cdot\frac{\partial}{\partial H}e^{-\beta H}) - \frac{1}{Z^2}(\sum\frac{\partial H}{\partial h}\cdot\frac{\partial}{\partial H}e^{-\beta H})(\sum se^{-\beta H}) \\ &= \frac{N\beta}{Z}\sum s^2e^{-\beta H} - \frac{1}{Z^2}(\beta\sum Nse^{-\beta H})(\sum se^{-\beta H}) \\ &= \frac{N}{k_BT}\{\frac{1}{Z}\sum s^2e^{-\beta H} - \frac{1}{Z^2}(\sum se^{-\beta H})^2\} \\ &= \frac{N}{k_BT}(\langle s^2\rangle - \langle s\rangle^2).\end{aligned} \tag{14}$$

2.5.1 Exercise 2.5.1

1. Intuitively explain why simple sampling is inefficient.

When N is large, the state space is also large, requiring an enormous number of samples to adequately cover it, making the calculation inefficient. Simple sampling treats all states equally, but in reality, there are physically important states. Since random samples are drawn from the state space, it becomes difficult to efficiently sample the important states. If these important states are overlooked, the calculation of the expected values of physical quantities may be inaccurate. In the Ising model, the behavior of physical quantities changes significantly near the phase transition point. Simple sampling struggles to capture the behavior in these critical regions, resulting in inefficiency.

2. Show that $W(x, x') = \min\{1, \frac{\rho(x')}{\rho(x)}\}$ satisfies $W(x, x')\rho(x) = W(x', x)\rho(x')$.

When $\rho(x') > \rho(x)$, $W(x, x') = 1$, $W(x', x) = \frac{\rho(x)}{\rho(x')}$. Therefore, $W(x, x')\rho(x) = W(x', x)\rho(x')$.

Conversely, when $\rho(x') < \rho(x)$, $W(x, x') = \frac{\rho(x')}{\rho(x)}$, $W(x', x) = 1$. Therefore, $W(x, x')\rho(x) = W(x', x)\rho(x')$.

3. For $N = 4^2$, $k_BT = 0.5, 5$ (using $J = 1$ as a unit), measure s and $|s|$ up to 200 MCS, and observe how they change as functions of MCS.

For zero external field ($h = 0$), the changes in s and $|s|$ at $k_BT = 0.5$ and 5 are shown in Figure 16, left and right, respectively. From the figure, at low temperatures, all spins quickly become -1, and s and $|s|$ converge rapidly, while at high temperatures, individual spins are unstable, causing s and $|s|$ not to converge.

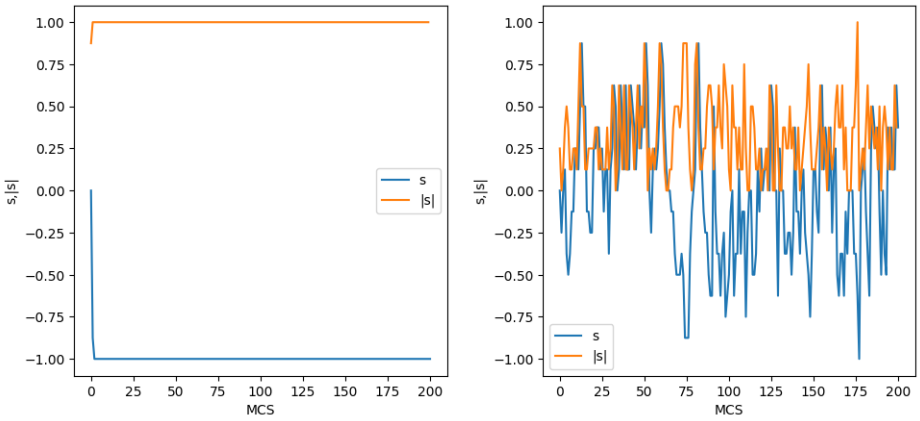

Figure 16: Changes in s and $|s|$ at $k_BT = 0.5$ (left) and 5 (right)

4. Measure magnetization, susceptibility, internal energy, and specific heat as functions of temperature, and estimate the transition point T_c (around $k_BT = 1.5 \approx 3$). For future reference, record $M = \langle s \rangle, M' = \langle |s| \rangle, \langle s^2 \rangle, \langle s^4 \rangle, \langle H \rangle, \langle H^2 \rangle$.

With a size of 6×6, measurements were averaged over the last 2000 MCS after running for 20000 MCS. The changes in magnetization ($M = \langle s \rangle, M' = \langle |s| \rangle$), susceptibility ($\chi$), internal energy ($u$), and specific heat ($c$) as functions of temperature are shown in Figure 17. From the figure, the transition temperature k_BT_c is estimated to be between 2.2 and 2.3. Near the transition point, if the temperature is lower than the transition point, susceptibility and specific heat increase, and the expected value of average magnetization ($\langle s \rangle$) becomes ± 1, indicating instability. On the other hand, if the temperature is higher than the transition point, susceptibility and specific heat decrease, and the expected value of average magnetization stabilizes at 0, as does the expected value of the absolute average magnetization. Internal energy increases monotonically with increasing temperature.

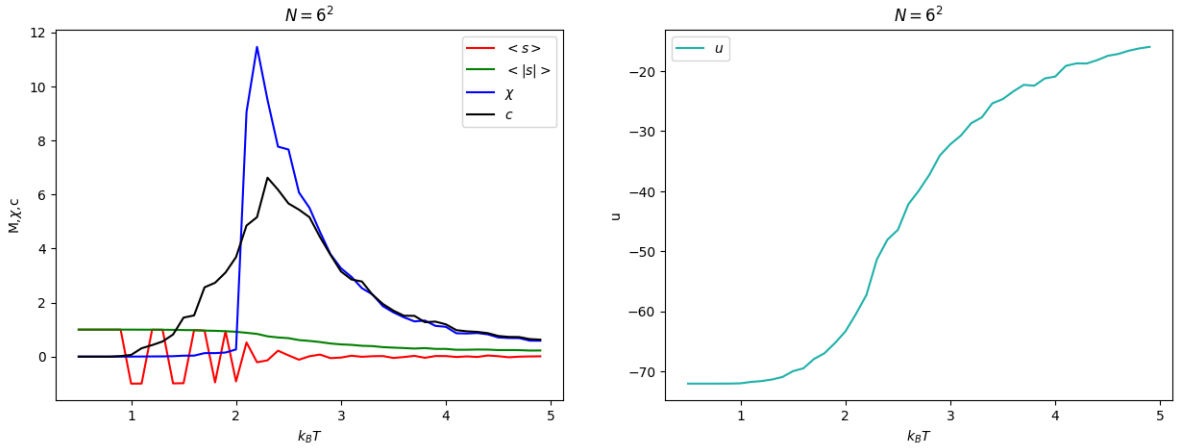

Figure 17: Temperature dependence of $M = \langle s \rangle, M' = \langle |s| \rangle, \chi, u, c$ for $N = 6^2$

5. Perform the same measurements for several lattice sizes and discuss the differences caused by the size.

For $N = 4^2, 8^2, 10^2$, the temperature dependence of the measurements mentioned above after 20000 MCS is shown in Figures 18 to 20, respectively. From Figures 17 to 20, it is found that as the size N increases, the estimation of the transition point becomes more accurate, the values of susceptibility and specific heat increase, internal energy decreases, and the expected value of average magnetization ($\langle s \rangle$) becomes less sensitive to temperature changes.

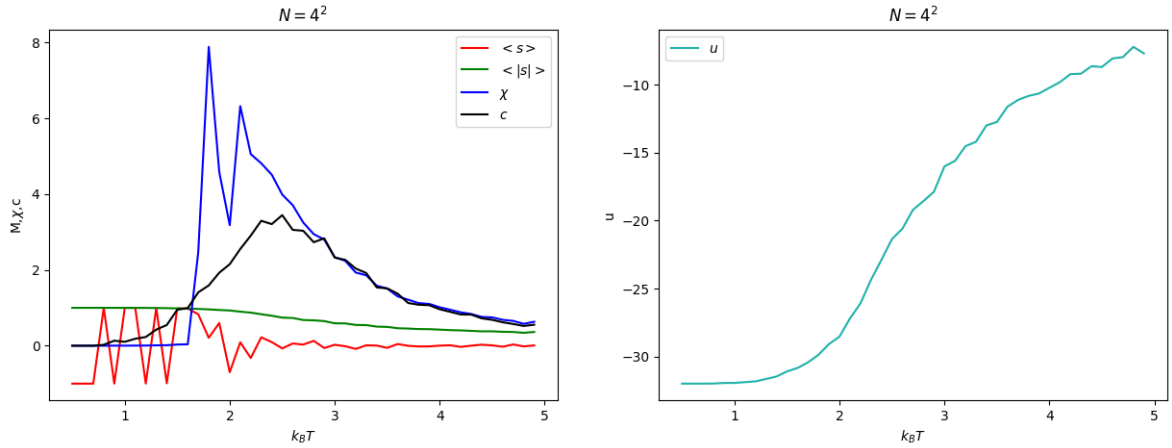

Figure 18: Temperature dependence of $M = \langle s \rangle, M' = \langle |s| \rangle, \chi, u, c$ for $N = 4^2$

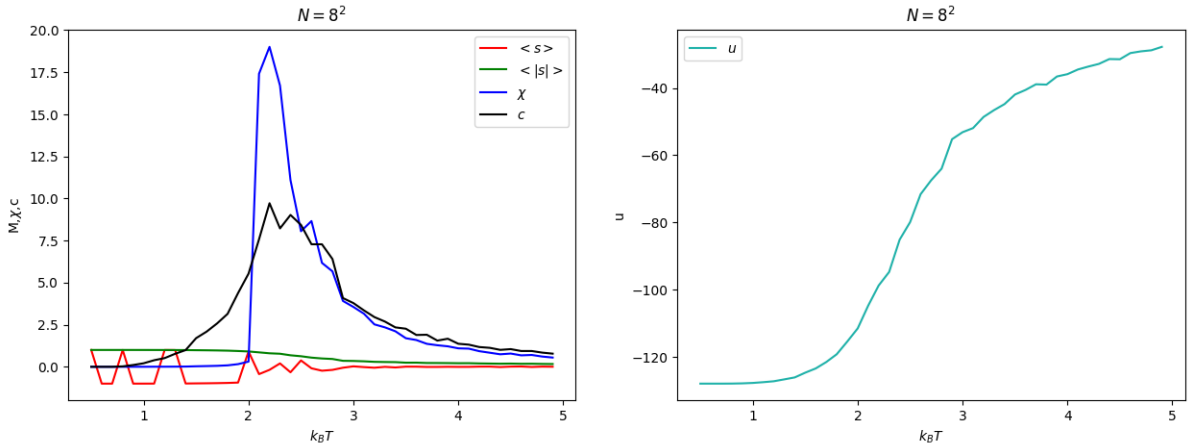

Figure 19: Temperature dependence of $M = \langle s \rangle, M' = \langle |s| \rangle, \chi, u, c$ for $N = 8^2$

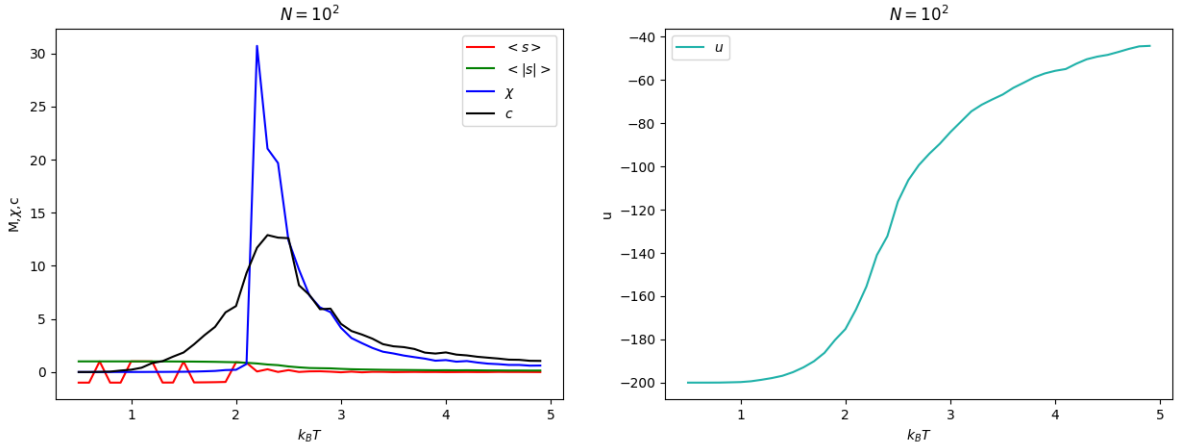

Figure 20: Temperature dependence of $M = \langle s \rangle, M' = \langle |s| \rangle, \chi, u, c$ for $N = 10^2$

2.5.3 Exercise 2.5.3

1. Use the Binder parameter to accurately determine T_c.

With MCS=30000 and $N = 6^2, 8^2, 10^2$, the average of the last 5000 MCS results gives the temperature dependence of the Binder parameter $U_L(T) = 1 - \frac{\langle s^4 \rangle_L}{3(\langle s^2 \rangle_L)^2}$, as shown in Figure 21. At $T = T_c$, $U_L(T)$ takes a constant value U^* independent of L, so the common intersection point of the graph indicates T_c. From the figure, $k_B T_c = 2.2J$, meaning the critical temperature T_c is $\frac{2.2}{k_B} K$.

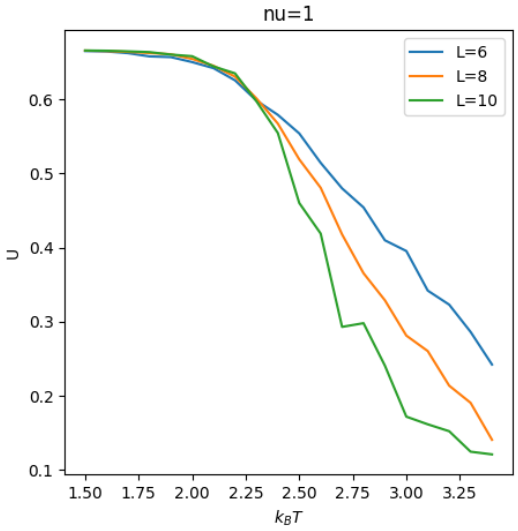

Figure 21: Temperature dependence of Binder parameter for $N = 6^2, 8^2, 10^2$

2. Analyze the size dependence of data just above the transition point to find β/ν and γ/ν.

Assuming the theoretical critical temperature $k_BT_c = 2.269$, MCS is 30000 for $L = 4$, increasing by 1000 for each increment of L, reaching MCS=36000 for $L = 10$. The change of $\log\langle|s|\rangle$ and $\log\langle\chi'\rangle$ with size L ($N = L^2$) is shown in Figure 22. The slopes are -0.112 and 1.790, respectively. Therefore, since $\langle|s|\rangle_{L,T} = L^{-\beta/\nu}\tilde{M}(L/\xi)$ and $\langle\chi'\rangle_{L,T} = L^{\gamma/\nu}\tilde{\chi}'(L/\xi)$, we have $\beta/\nu = 0.112$ and $\gamma/\nu = 1.790$, which are close to the theoretical values of $\beta/\nu = 0.125$ and $\gamma/\nu = 1.75$.

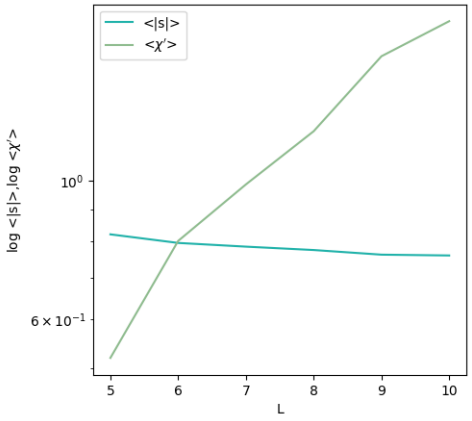

Figure 22: Size dependence of $\log\langle|s|\rangle$ and $\log\langle\chi'\rangle$ with L ($N = L^2$)

3. Plot $\tilde{M}$ with the x-axis as $|T - T_c| \times L^{1/\nu}$ and the y-axis as $ML^{\beta/\nu}$. Similarly, plot $\tilde{\chi}'$ with the x-axis as $|T - T_c| \times L^{1/\nu}$ and the y-axis as $\chi' L^{-\gamma/\nu}$. Determine the value of ν such that all size data falls on the same curve.

When $\nu = 1$, plotting $\tilde{M}$ with the x-axis as $|T - T_c| \times L^{1/\nu}$ and the y-axis as $ML^{\beta/\nu}$ gives the graph shown on the left in Figure 23. Plotting $\tilde{\chi}'$ with the x-axis as $|T - T_c| \times L^{1/\nu}$ and the y-axis as $\chi' L^{-\gamma/\nu}$ gives the graph shown on the right in Figure 23. From the figures, it is clear that $\nu = 1$.

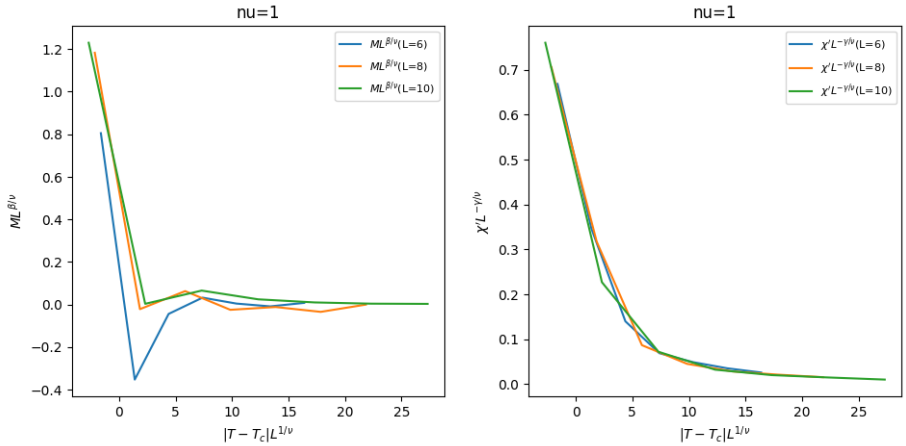

Figure 23: Graphs of $\tilde{M}$ (left) and $\tilde{\chi}'$ (right) for $\nu = 1$

To verify this, the same measurement was performed with $\nu = 1.5$, as shown in Figure 24, indicating that the value of ν is not appropriate.

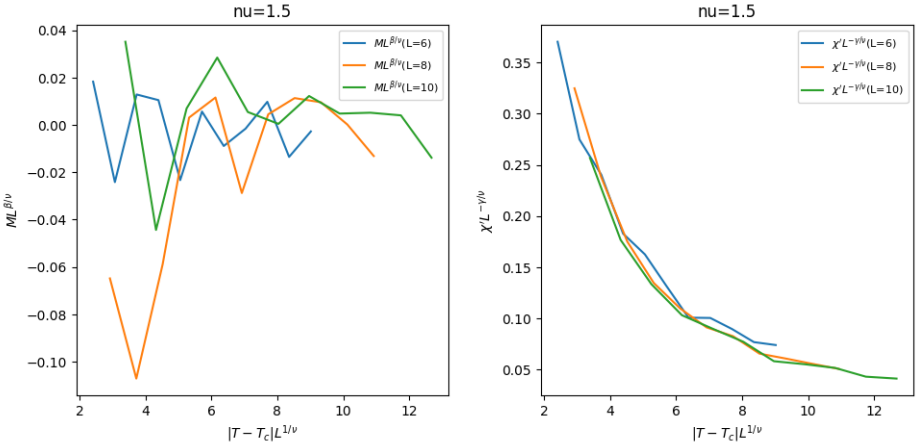

Figure 24: Graphs of $\tilde{M}$ (left) and $\tilde{\chi}'$ (right) for $\nu = 1.5$

4. Investigate other boundary conditions (e.g., free boundary).

For the free boundary condition, the temperature dependence of the Binder parameter is shown in Figure 25, and the transition point is estimated to be around 2.3 to 2.4. Setting up as in Problem 2 (changing periodic boundary to free boundary), the size dependence of $\log\langle|s|\rangle$ and $\log\langle\chi'\rangle$ is shown in Figure 26, with slopes of -0.0135 and 0.0015, respectively. Therefore, under the free boundary condition, $\beta/\nu = 0.0135$ and $\gamma/\nu = 0.0015$, which deviate from the theoretical values.

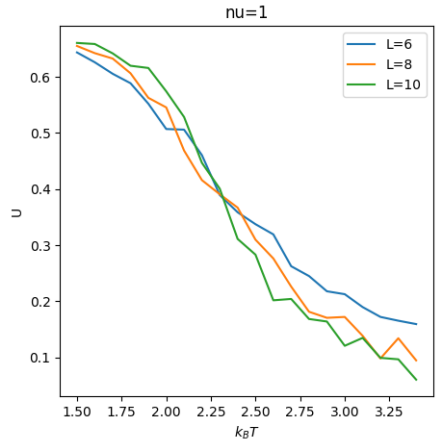

Figure 25: Temperature dependence of Binder parameter for $N = 6^2, 8^2, 10^2$ (free boundary)

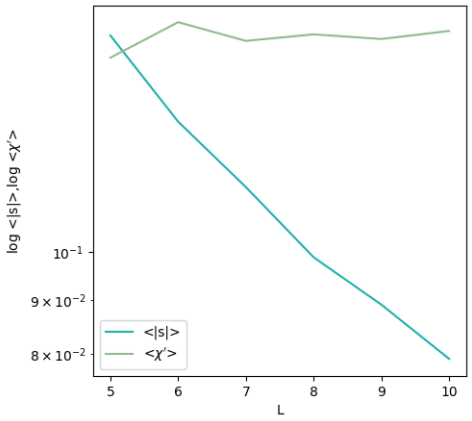

Figure 26: Size dependence of $\log\langle|s|\rangle$ and $\log\langle\chi'\rangle$ with L ($N = L^2$) (free boundary)

5. Under the finite size scaling hypothesis, show that $\frac{1}{\nu} = \frac{\log(\frac{dU_{bL}}{dU_L})}{\log b}\,|_{U_\star}$, $\frac{\gamma}{\nu} = \frac{\log(\chi(bL)/\chi(L))}{\log b}\,|_{T_c}$. Use this to find $1/\nu$ and γ/ν. Specifically, for a fixed L, plotting with the x-axis as $1/\log b$ and the y-axis as $\frac{\log(\frac{dU_{bL}}{dU_L})}{\log b}\,|_{U_\star}$ should yield a straight line. Ideally, when plotting such lines for all L, they should intersect at $1/\log b = 0$.

With $L = 10$ and $b = 3, 4, 5$, calculating $\frac{dU_{bL}}{dU_L}$ by computing $\frac{dU_{bL}}{dT}$ and $\frac{dU_L}{dT}$ at two points gives

$$\frac{1}{\nu} = \frac{\log(\frac{dU_{bL}}{dU_L})}{\log b}\,|_{U_\star} = \frac{\log(\frac{dU_{bL}}{dT}/\frac{dU_L}{dT})}{\log b}\,|_{U_\star} \approx 3 \tag{15}$$

Meanwhile, γ/ν is also calculated to be around 1.8.

3 Independent Research: Traffic Congestion

3.1 Introduction

Traffic science is a field of traffic engineering that studies the design, management, control, and optimization of traffic. In traffic science, the cellular automaton model is often used, which involves modeling traffic congestion using a lattice of cells and simple rules. There are various types of cellular automaton models, such as Rule 184, ASEP, Quick-Start model, and Slow-Start model, but this study will focus on the Rule 184 and ASEP models. The basic condition in this study is that only one vehicle can occupy one cell, and periodic boundary conditions are used.

Next, variables are defined. In traffic science, flow is defined as the total number of vehicles passing a certain point within a certain time, and in this study, it will be defined as the number of vehicles passing a certain point (or multiple points) within a fixed number of steps. Speed is defined as the number of vehicles passing a certain point (or multiple points) within a fixed number of steps divided by the total number.

3.2 Rule 184

Rule 184 is the simplest of the cellular automaton models. According to the rule, if the cell in front is empty, the vehicle moves forward in the next step; if the cell in front is occupied, the vehicle cannot move in the next step.

3.2.1 1-Dimensional

In a 1-dimensional road of length 100, after running 1000 steps, the average of the last 100 data points is taken for each value. At each step, if there is a vehicle in front of an empty cell, it moves to the empty cell. That is, in each step, every vehicle that can move forward by one cell does so. The flow and speed changes concerning density, with a maximum vehicle speed of 1, are shown in Figure 27. The red graph represents the theoretical curve, indicating the total number of vehicles that can move forward in one step, while the blue graph shows the actual flow measured at $x = 50$. The graph shows that the flow increases monotonically with the number of vehicles, but when the density reaches 0.5 ($= \frac{\text{number of vehicles}}{\text{total}}$), the critical density is reached, resulting in a phase transition. When the density exceeds the critical density, the flow decreases monotonically as the number of vehicles increases. The reason for the difference between the actual flow and the theoretical curve is that when there are few vehicles, the flow increases proportionally to the number of vehicles, but as it approaches the critical density, it gradually "saturates," and the acceleration of the flow increase becomes negative. The shape of the graph above the critical density suggests that as the density approaches the true saturation state (maximum number of vehicles), the acceleration of the density decrease also becomes negative. Meanwhile, the theoretical speed remains constant until the density reaches the critical density, after which it decreases monotonically as density increases. However, in practice, speed decreases monotonically from the start. This difference arises from the distinction between macroscopic and microscopic phenomena; that is, while the overall speed does not change until the critical density is reached, it decreases when observed from a specific point.

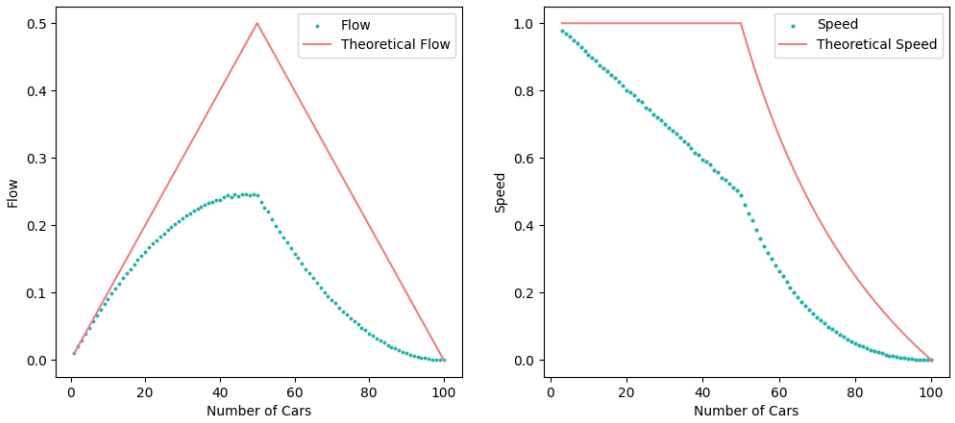

Figure 27: Flow and Speed Changes Concerning Density in 1-Dimensional Case

3.2.2 2-Dimensional

In a 100×100 grid, 20 roads are placed at equal intervals at $x = 5, 15, \cdots, 85, 95$ and $y = 5, 15, \cdots, 85, 95$. The intersections at points where x and y meet (e.g., (15,15)) become intersections, resulting in 100 intersections in the grid. Vehicles at intersections continue in the same direction, following Rule 184.

After running 1000 steps, the flow and speed changes concerning density are shown in Figure 28. The red graph represents the theoretical curve, while the blue graph shows the actual flow's (4th-order) regression curve. The graph shows that the 2-dimensional flow change has a similar trend to the 1-dimensional case, with a critical density still around $\frac{1}{2}$, but the regression curve leans to the left compared to the theoretical curve. In the 1-dimensional case, a vehicle can only be stopped by the vehicle in front of it, but in the 2-dimensional case, vehicles coming from other directions at intersections can also stop it. This increases the likelihood of a vehicle stopping, reducing the critical density.

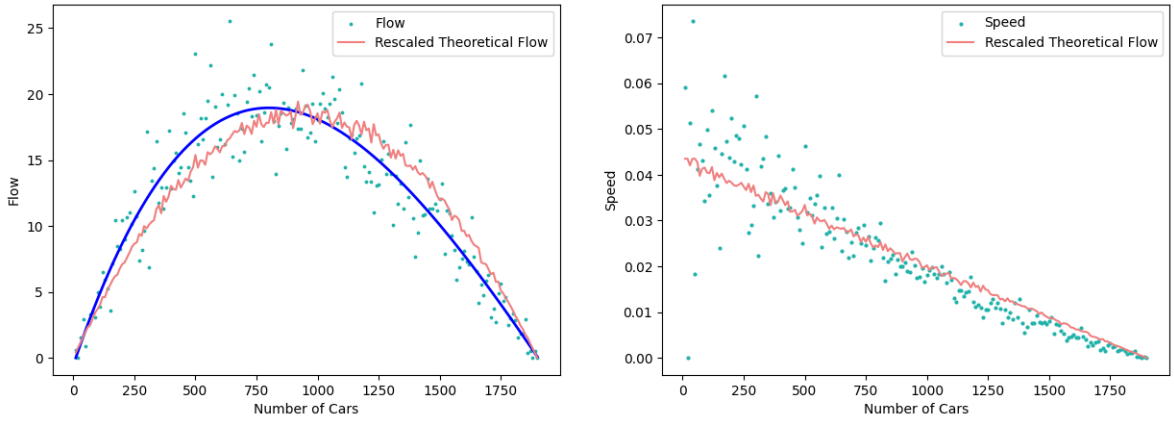

Figure 28: Flow and Speed Changes Concerning Density in 2-Dimensional Case

3.3 ASEP

The ASEP model is a simple mathematical model that models particle movement on a one-dimensional lattice and is used to study various phenomena such as traffic congestion and material flow. The original ASEP model allows particles to move left or right on a one-dimensional lattice with a certain probability, but when studying traffic congestion, vehicles can only move in one direction. Therefore,

the ASEP model is modified to allow vehicles to move forward with probability p if the cell in front is empty. In this study, the model is extended to 2 dimensions, with the same rules at intersections.

3.3.1 1-Dimensional

The operation is similar to Rule 184, except that vehicles move forward with probability p if the cell in front is empty.

The flow and speed changes concerning density for $p = 0.8, 0.5, 0.3, 0.1, 0.05, 0.01$ are shown in Figures 29∼34. The graphs show that when p is large, it resembles the Rule 184 graph. As p decreases, the unpredictability of flow increases when there are few vehicles. However, as p decreases further, the flow becomes gradually predictable. When p is large, the probability of moving forward is high, reducing uncertainty. As p decreases (to 0.5), the uncertainty of moving forward increases, making flow prediction difficult. However, when $p < 0.5$, vehicles are more likely to stop than to move forward, regardless of whether the cell in front is empty. Therefore, as $p(< 0.5)$ decreases further, both flow and speed converge to 0.

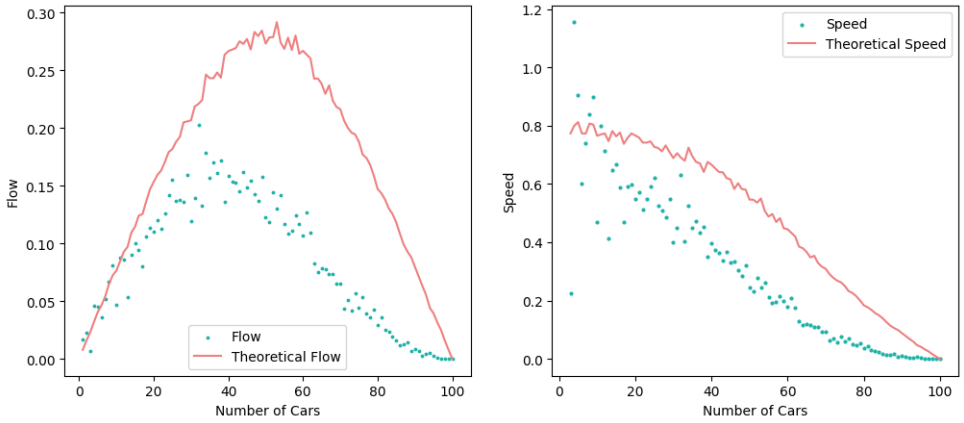

Figure 29: Flow and Speed Changes Concerning Density in 1-Dimensional Case ($p = 0.8$)

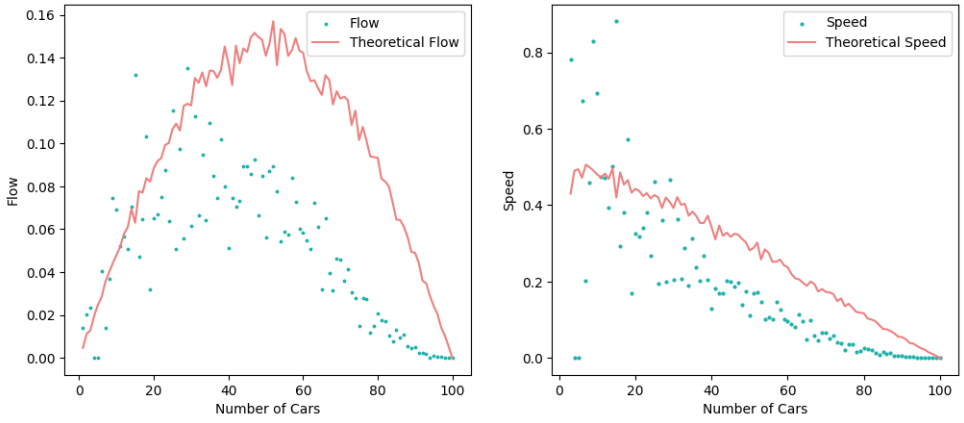

Figure 30: Flow and Speed Changes Concerning Density in 1-Dimensional Case ($p = 0.5$)

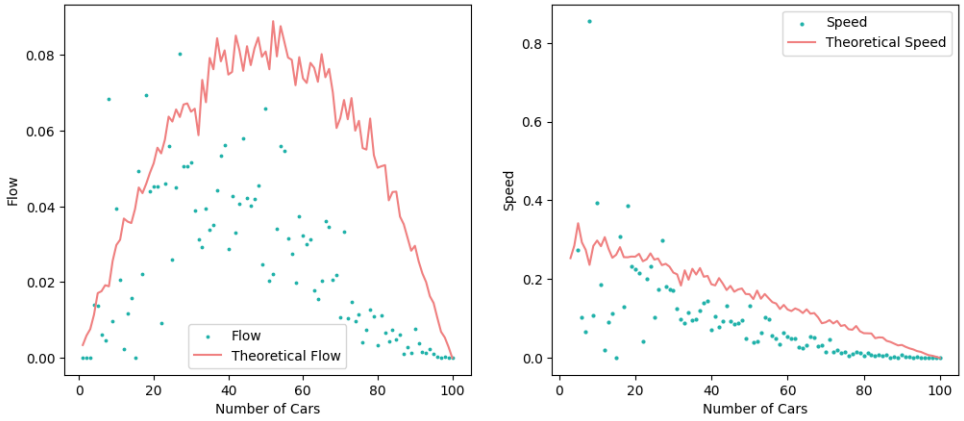

Figure 31: Flow and Speed Changes Concerning Density in 1-Dimensional Case ($p = 0.3$)

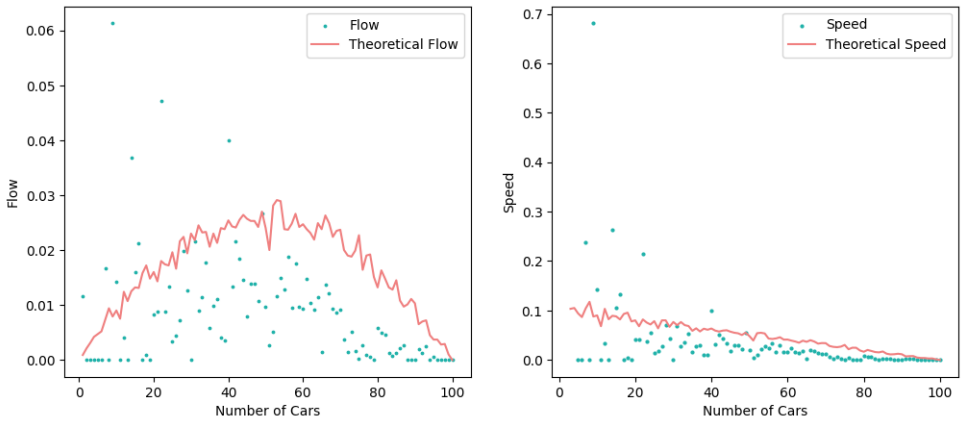

Figure 32: Flow and Speed Changes Concerning Density in 1-Dimensional Case ($p = 0.1$)

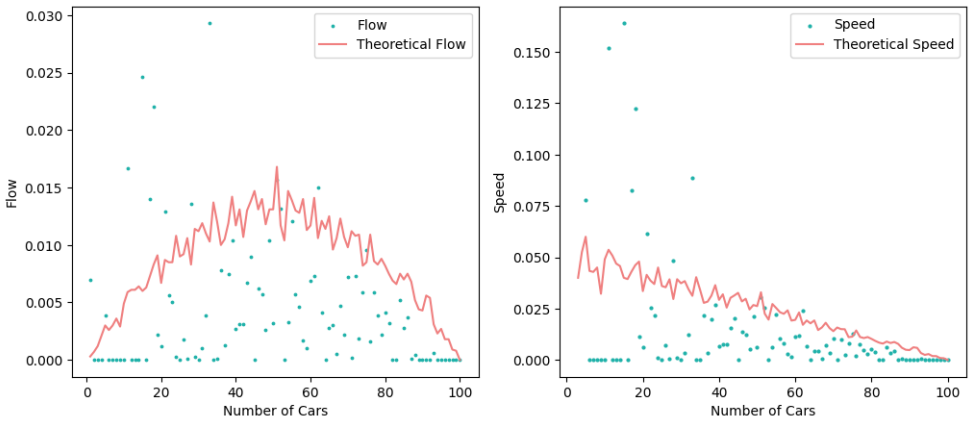

Figure 33: Flow and Speed Changes Concerning Density in 1-Dimensional Case ($p = 0.05$)

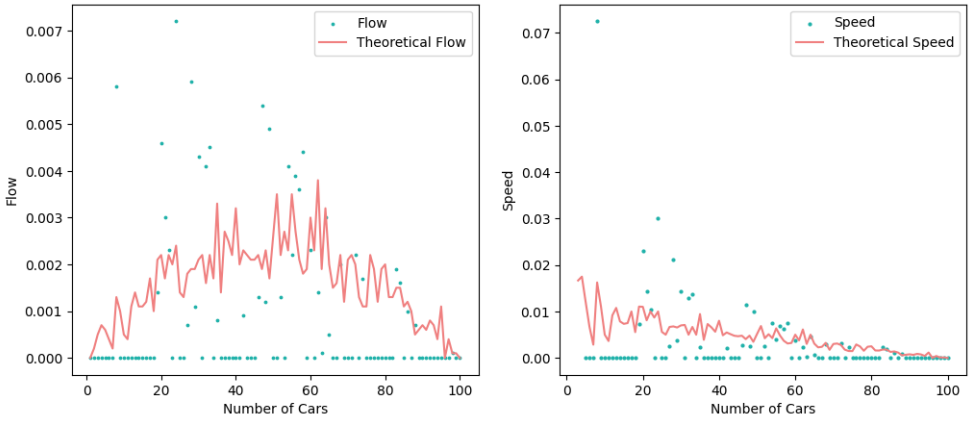

Figure 34: Flow and Speed Changes Concerning Density in 1-Dimensional Case ($p = 0.01$)

3.3.2 2-Dimensional

In the 1-dimensional case, the predictability of flow and speed decreases and then increases with increasing p in the ASEP model, but this is not the case in 2 dimensions. For $p = 0.8, 0.5, 0.1$, the flow and speed changes concerning density in 2 dimensions are shown in Figures 35∼37. The figures show that the shape of the graph remains unchanged as p decreases, with only the values becoming smaller. In the 1-dimensional case, vehicle movement is restricted only by the vehicle in front, so when the unpredictability of the forward vehicle's movement increases, so does the unpredictability of this vehicle's movement. Therefore, flow and speed in 1 dimension are strongly affected by p. On the other hand, in 2 dimensions, there are more restrictions on vehicle movement. For example, a vehicle moves to $x = 54, y = 15$, and in the next step (moving right), it reaches an intersection. At the intersection, this vehicle is influenced not only by the vehicle in the same direction but also by the vehicle on the right (at $x = 55, y = 14$). Thus, even if the unpredictability of movement in the same direction and the right direction is high, this vehicle cannot move if the vehicle in the same direction stops or the vehicle on the right moves forward. Therefore, in 2 dimensions, the greater restrictions at intersections compared to 1 dimension reduce the unpredictability of flow and speed changes.

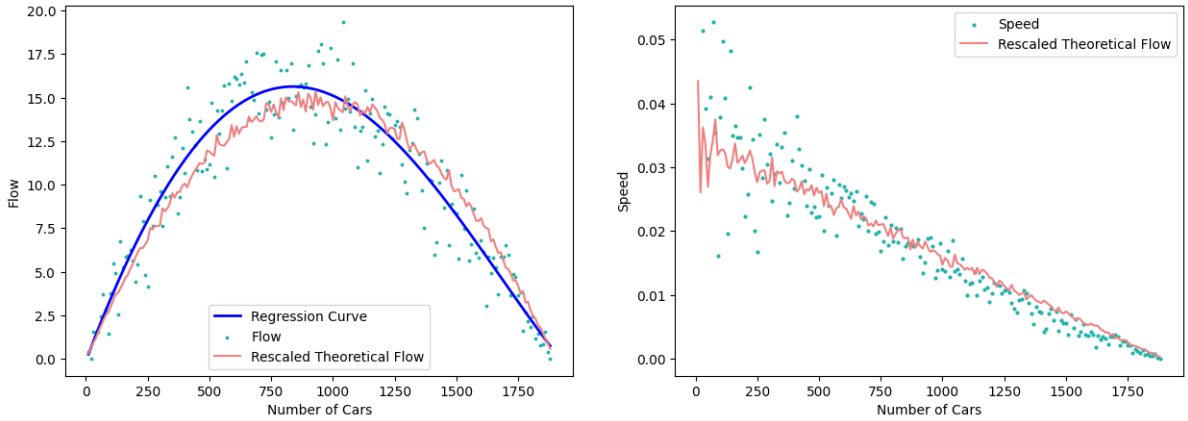

Figure 35: Flow and Speed Changes Concerning Density in 2-Dimensional Case ($p = 0.8$)

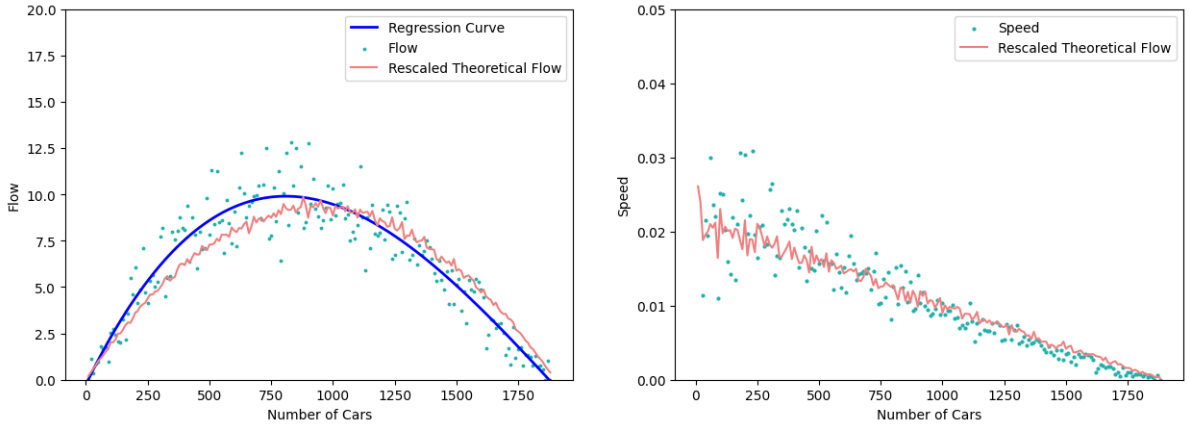

Figure 36: Flow and Speed Changes Concerning Density in 2-Dimensional Case ($p = 0.5$)

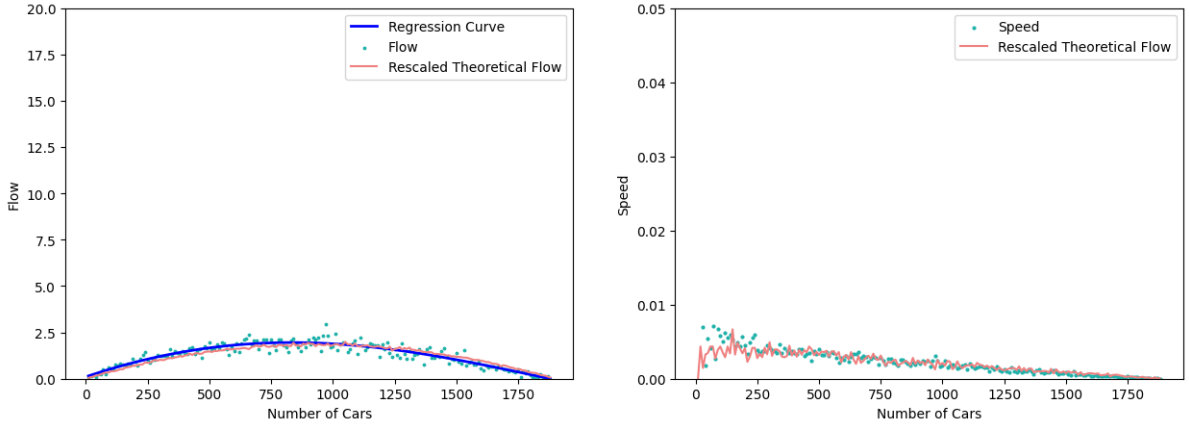

Figure 37: Flow and Speed Changes Concerning Density in 2-Dimensional Case ($p = 0.1$)